High Quantum Yield Fluorescent Carbon Nanodots for Detection of Fe(III) Ions and Electrochemical Study of Quenching Mechanism

By: Durga M. Arvapalli, Alex T. Sheardy, Kalyan C. Alapati, and Jianjun Wei

D. Arvapalli, A. Sheardy, K. Alapati, J. Wei High Quantum Yield Fluorescent Carbon Nanodots for Detection of Fe(III) Ions and Electrochemical Study of Quenching Mechanism, *Talanta*, **2020**, 209, 120538. DOI: 10.1016/j.talanta.2019.120538.

Abstract:

Carbon nanodots (CNDs) offer potential applications in photocatalysis, optoelectronics, bio-imaging, and sensing due to their excellent photoluminescence (PL) properties, biocompatibility, aqueous solubility, and easy functionalization. Recent emphasis on CNDs in the selective detection of metal ions is due to the growing concern for human and environmental safety. In this work, two types of fluorescent carbon nanodots (CNDs) are synthesized economically from ethylene diamine (E-CNDs) or urea (U-CNDs) in a single step microwave process. The as-prepared CNDs exhibit excellent PL at an excitation wavelength of 350 nm with a quantum yield of 64% for E-CNDs and 8.4% for U-CNDs with reference to quinine sulfate. Both E-CNDs and U-CNDs demonstrate high selectivity towards Fe (III) ions among different metal ions, by fluorescence quenching in a dose dependent manner. The limit of detection of E-CNDs and U-CNDs is observed to be 18 nM and 30 nM, respectively, in the linear response range of 0–2000 μM with a short response time (seconds). The CNDs detect Fe (III) ions in tap water and serum sample with no spiking and the recovery was ~100% with the Fe (III) samples. Cellular internalization studies confirm the localization of the CNDs and the optical imaging sensing of Fe (III) ions inside living cells. A charge transfer fluorescence quenching mechanism, specifically between the CNDs and Fe (III), is proposed and examined using cyclic voltammetry. The overall characteristics of the E-CNDs provides a potential sensing platform in highly sensitive and selective detection of Fe (III) ions.

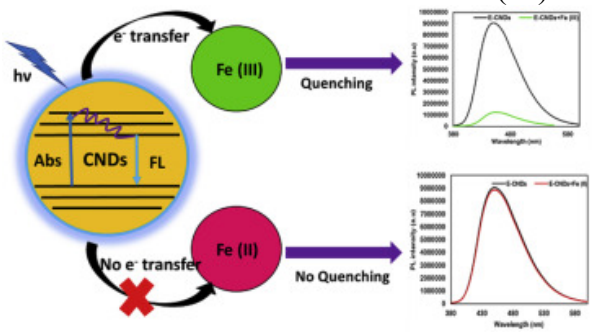

Keywords: Carbon nanodots | Fluorescence quenching | Iron ion detection | Electrochemistry | Charge transfer

Article:

1. Introduction

Metal ions are an integral part in various biological and biochemical processes [1]. Iron is an essential micronutrient for the human body and most biological electron transfer processes rely on iron proteins [2]. Fe^{3+} is a major component of hemoglobin that facilitates oxygen transport in blood [3]. Iron deficiency in pregnant women have increased risk of anemia and sepsis associated with high mortality and morbidity rates [4]. Moreover, iron plays an important role in brain development of new born babies [5], body temperature regulation [6], and muscle function [7]. Also, overload of iron may lead to neurological diseases such as Parkinson's and Alzheimer's [8]. Current detection techniques such as atomic absorption spectrometry and ion chromatography rely on the use of complicated sample preparation and instrumentation [9]. Therefore, monitoring of iron levels is challenging and detection with high sensitivity and selectivity is of great importance.

Use of fluorescent materials in the sensitive detection of biologically important metal ions has tremendous potential in the field of biomedicine [10]. Quantum dots and organic fluorescent dyes, due to their high quantum yield, are used widely as contrast agents for detection [11]. However, irreversible photobleaching and low optical absorption cross-section renders the limitation of the organic dyes in detection. Quantum nanoparticles have replaced the usage of organic dyes due to their broad absorption spectra [12] and quantum confinement effect [11], but their instability [13] and the presence of toxic heavy metals limits their applications for detection in living cells [14,15]. Moreover, despite all the recent advancements in the field of biosensing, development of sensitive and selective fluorescence detection of Fe (III) ions is still a challenge. With this regard, effort has been taken in search of small nanoparticles [16,17] with better defined PL [18], higher quantum yield [19], and good biocompatibility for the detection of biologically significant metal ions [20]. Fluorescent carbon nanodots (CNDs) in the nanocarbon family offer superior aqueous solubility [18], robust chemical inertness, promising PL properties [21] and better biocompatibility than heavy metal quantum dots [22,23]. Moreover, polarized carbon atoms [24] and oxygen containing functional groups such as hydroxyl and carboxyl groups in the CNDs contribute to the overall hydrophilicity providing a better platform for easy functionalization of various organic, inorganic, and biological entities [[25], [26], [27], [28]]. High sensitivity, short response time, stable PL, and low toxicity [29] of the CNDs provides a suitable platform for biosensing [30].

In recent years, several reports have been focused on detection of iron using CNDs. These studies have shown that nitrogen-doping can effectively enhance fluorescence quantum yield, resulting in high sensitivity and rapid response [[31], [32], [33], [34], [35], [36], [37]]. Various CNDs exhibited sensitivity towards iron with limits of detection confined to ppm levels [38,39], however increasing the quantum yield could result in even more sensitive detection. Few reports demonstrated limit of detection (LOD) in nanomolar range using CNDs of a good quantum yield

[[40], [41], [42]]. Moreover, multiple researchers have synthesized biocompatible CNDs that enable cell imaging along with iron sensing [40,[43], [44], [45], [46], [47]]. Despite all the recent advancements, there is still a need for the economical synthesis of an appropriate nanoprobe that offers high quantum yield, and improved sensitivity and selectivity. Additionally, the underlying detection mechanism is less studied and needs to be explored.

Hydrothermal method or microwave-assisted CND synthesis has been well established to doping different elements thus tuning the quantum yield [[48], [49], [50], [51], [52], [53]]. Herein we use a facile, cost effective, one-step microwave synthesis of highly fluorescent, small, water-soluble CNDs using two different precursor molecules, ethylene diamine (EDA) for E-CNDs and urea for U-CNDs for a comparison study. The CNDs are well characterized and then used in the Fe (III) detection studies. The as synthesized E-CNDs showed the LOD of 18 nM with a quantum yield of 64% by incorporating a high amount of nitrogen (11–12%), comparable to previously nitrogen doped CNDs-based sensing probes for iron detection [32,36,37,54]. Upon addition of Fe (III) ions, the fluorescence intensity of the CNDs was quenched with a fast response time within 1 min. The quenching of the CNDs upon addition of Fe (III) was evaluated using the Stern-Volmer equation. Iron (III) detection in real samples such as tap water and human serum was performed as an application demonstration. Moreover, optical imaging of human endothelial (EA. Hy926) cells with Fe (III) incubation shows potential of using CNDs for iron sensing in living cells. The current work demonstrates high quantum yield CNDs as a fluorescence turn off sensor in the detection of Fe (III) with improved selectivity, fast response time, and better limit of detection than traditional methods. Moreover, to further understand the quenching reaction of CNDs by Fe (III), which is inadequately studied, an electrochemical technique, cyclic voltammetry, was used to investigate the charge transfer between the CNDs and Fe (III) by changing the concentration of CNDs in the Fe (III) solutions.

2. Experimental

2.1. Materials

Citric acid (ACROS Organics), Urea (Aldrich, 99% ACS reagent), Ethylenediamine (EDA, Fisher Scientific), quinine sulfate dihydrate, KCl (ACROS Organics), $CoCl_2$, $FeCl_2$ (Alfa Aesar), $FeCl_3$, $CrCl_3$, $AgNO_3$, $CuCl_2$, $CaCl_2$, $MgCl_2$, gold electrode, Ag/AgCl reference electrode, platinum electrode (Fisher Scientific), DMEM media, EA. hy926 cell line (ATCC), pen/strep solution, fetal bovine serum (Sigma Aldrich), CCK-8 assay kit (Sigma Aldrich), human serum. These materials were used in the present work without any further purification.

2.2. Synthesis of CNDs

Fluorescent CNDs (E-CNDS & U-CNDs) were synthesized through a microwave-assisted procedure. Briefly, 960 mg of citric acid (ACROS Organics) was mixed with 1 ml EDA and 1 ml of DI water, and pyrolyzed in microwave synthesizer (CEM Corp 908005 Microwave Reactor) for 18 min at temperature below 150 °C and 300 W power to synthesize E-CNDs. The brown foamy solution was dissolved in 5 ml of DI water and dialyzed through MWCO 1000 membrane (Scientific Fisher) for 24 h. Similarly, U-CNDs were synthesized by mixing 1 g of urea with 1 g of citric acid and 1 ml of DI water and pyrolyzed in 150 W microwave for 12 min at 110°c. The

U-CNDs were dialyzed in the same way as done for E-CNDs. The cooled reactant mixture was centrifuged at 3500 rpm for 20 min to remove large and aggregated particles. The two CNDs solutions were freeze dried for 24 h using a freeze drier (Labconco Free Zone 6 Freeze Dryer).

2.3. CNDs characterization

The synthesized CNDs were characterized using Transmission Electron Microscopy (TEM, Carl Zeiss Libra 120 Plus). The CNDs were dropped onto carbon coated copper grids for analysis. The size was further characterized using Atomic Force Microscopy (AFM, Agilent 5600LS AFM) in tapping mode. AFM samples were prepared by dropping CND solutions onto a freshly-cleaved mica surface and vacuum dried. Fourier transform infrared (FTIR) spectroscopy (Agilent FTIR) was used to investigate surface functional groups. XPS (Thermo Scientific ESCALAB Xi^+) and EDX (Bruker Nano XFlash Detector 5030) were used to determine elemental composition and atomic weight % of the as prepared CNDs. Zeta potential of the CNDs (0.05 mg mL^{-1}) was measured using Malvern Zetasizer ZEN3600. The optical properties of the CNDs were measured using UV–Visible spectroscopy (Varian Cary 6000i) and fluorescence spectroscopy (Horiba FluoroMax-4). Excitation-dependent behavior of the as prepared E-CNDs (0.01 mg mL^{-1}) and U-CNDs (0.1 mg mL^{-1}) was determined using a fluorescence spectrophotometer at different excitation wavelengths ranging from 330 to 450 nm.

2.4. Fluorescence quantum yield (QY) measurement

The fluorescence quantum yield of the as synthesized CNDs was measured with Quinine Sulfate (QS) in 0.1 M H_2SO_4 as a standard (QY: 54%) using the following equation [53,55,56]:

$$\Phi C = \Phi QS \times \frac{GradC}{Grad\ QS} \times \frac{\eta C2}{\eta QS2} \quad (1)$$

where, Φ represent the quantum yield, Grad is the gradient from the plot of integrated fluorescence intensity vs absorbance and η, refractive index (aqueous solution 1.33); the plots of E-CNDs and U-CNDs as a comparison to the standard QS are shown in Fig. S1, respectively. The subscript QS and C denoted quinine sulfate and CNDs respectively.

2.5. Time dependent detection of Fe (III) ions with CNDs

The decrease in the fluorescence intensity of the CNDs with addition of Fe (III) ions was carried out for different time intervals ranging from 0.5, 1, 2, 3, 4, 5, 6, 7, 8, 9, 10, 15 min. A 10 µl aliquot of each types of E-CNDs (0.01 mg mL^{-1}) and U-CNDs (0.1 mg mL^{-1}) was suspended in 100 µl of Fe (III) (10 µM) and 890 µl of water. The fluorescence intensity was calculated for each time interval.

2.6. Stability and selective detection of Fe (III)

The stability of the CNDs in aqueous solution was measured for every 10 days up to 50 days using a fluorescence spectrophotometer. The selectivity of the CNDs towards Fe (III) ions was determined. Briefly, 50 µM of different metal ions (Ca^{2+}, Co^{2+}, Fe^{2+}, Ag^+, Cu^{2+}, K^+, Fe^{3+},

Cr^{3+} and Mg^{2+}) were mixed with 10 µl of E-CNDs (0.01 mg mL^{-1}) and U-CNDs (0.1 mg mL^{-1}). The selectivity of the CNDs towards Fe (III) in the presence of competitive metal ions was tested. The fluorescence spectra were measured for each type of the metal ions used.

2.7. Electrochemical Study

Cyclic voltammetry was performed using a three-electrode electrochemical cell with a working gold electrode, 3 M Ag/AgCl reference electrode and platinum counter electrode. The electrolyte solution is 10 mM Fe (III) ions with different concentrations of CNDs in nitrogen-purged deionized water. The samples were run at different scan rates at room temperature.

2.8. CNDs based sensing of Fe (III) in real samples

Human serum samples were centrifuged to remove protein content and the supernatant was treated with CNDs at a concentration of 0.1 mg mL^{-1} to detect the levels of Fe (III). Then the serum samples were spiked with different concentrations of Fe (III) and recovery rates were calculated based on the standard curve of the Fe (III). Briefly, 10 µl of E-CNDs (0.01 mg mL^{-1}), 10 µl of different concentrations of Fe (III) and 80 µl of human serum were mixed together and incubated for 5 min at room temperature and the emission spectra was recorded using an excitation wavelength of 350 nm. Similar set of experiments were performed with U-CNDs at a concentration of 0.1 mg mL^{-1}.

2.9. Intracellular uptake and optical imaging of the CNDs

Human endothelial cells (EA. Hy926) were cultured in DMEM supplemented with 10% FBS and 1% pen/strep antibiotic solution. The cells were seeded on sterilized glass cover slips in 24 well plates and incubated at 37 °C and 5% CO_2 for 24 h, followed by incubation with E-CNDs (0.2 mg mL^{-1}) or U-CNDs (0.5 mg mL^{-1}) for 6 h. The cells were washed twice with 1x PBS and treated with 10 µM Fe (III) in DMEM media for different time intervals (5 min, 30 min and 1 h). As a control, no Fe (III) ions were added. The cells were washed twice with 1x PBS and fixed with 4% paraformaldehyde for 12 min. The cells were washed twice with 1x PBS and stained with mitotracker green (stains actin filaments) 30 min. The cover slips were mounted on the glass slides using mounting media and imaged under confocal microscope (Zeiss Z1 Spinning Disk Confocal Microscope) at 20X magnification.

3. Results and discussion

3.1. Characterization of the CNDs

The AFM images show the even dispersion of E-CNDs (Fig. 1A) on the mica surface with an average height of 7 nm. Similarly, U-CNDs (Fig. 1C) also show an even distribution on the mica surface with an average height of 2.4 nm. Since both CNDs are smaller than the radius of curvature for the AFM probe, only the height data can be used to determine size. The TEM images demonstrate monodisperse, spherical E-CNDs (Fig 1B) and U-CNDs (Fig. 1D) with sizes around 7 nm and 2.4 nm, respectively, which are in accordance with the height profiles of the

AFM images. The overall yield of E-CNDs and U-CNDs was found to be 8% and 5%, respectively.

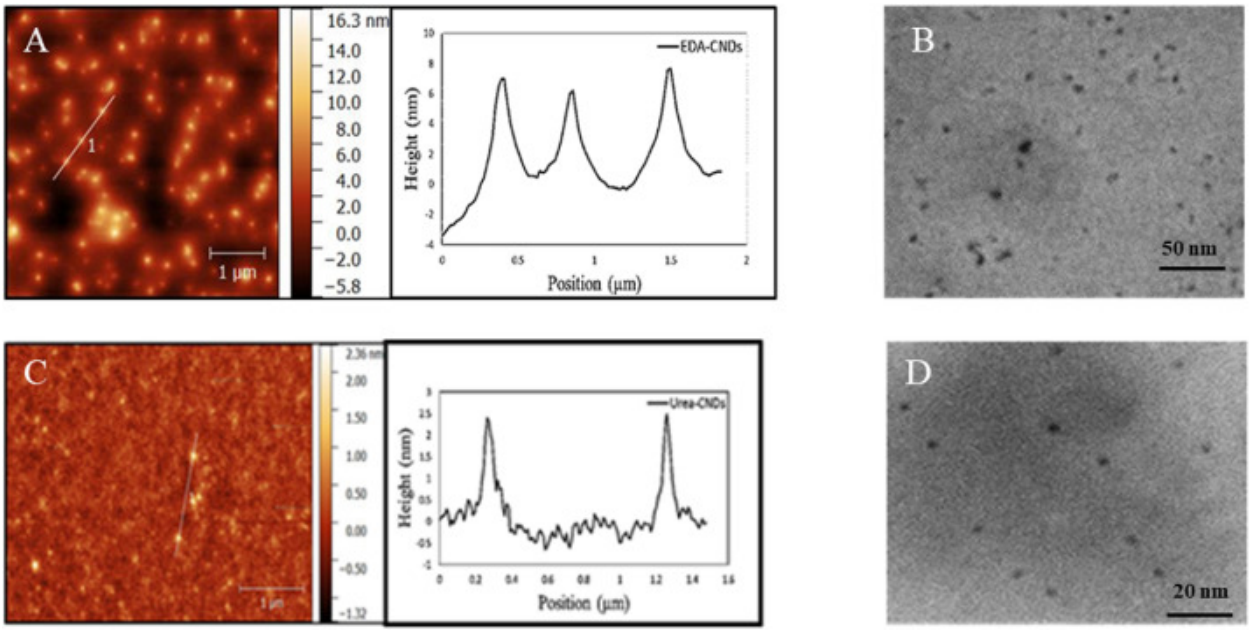

Fig. 1. Atomic force microscopy (AFM) images of E-CNDs (A) and U-CNDs (C) with their respective height profiles around 7 nm and 2.4 nm respectively, and the TEM images of E-CNDs (B) and U-CNDs (D), respectively.

The XPS survey spectra of both the E-CNDs (Fig. 2A) and U-CNDs (Fig. 2C) show the presence of peaks at 285.0, 400.5, and 532.0 eV attributing to C1s, O1s and N1s respectively. E-CNDs present an intense N1s peak (Fig. 2A) in comparison to the U-CNDs (Fig. 2C) depicting higher amounts of N incorporated into E-CNDs from EDA [57]. The C1s spectrum of U-CNDs (Fig. 2B) show C–C, O–C═O and C–O–C surface groups whereas E-CNDs (Fig. 2D) gives one more additional C–O functional group. The O1s and N1s spectra for both E-CNDs (Figs. S2A and S2B) and U-CNDs (Figs. S2C and S2D) are observed at 531 and 400 eV respectively. EDX analysis provides the weight and atomic ratios of C, H, O and N for both E-CNDs (Fig. S3A) and U-CNDs (Fig. S3B), and higher nitrogen content in E-CNDs (11.3% wt) vs. U-CNDs (8.2% wt) was observed. The reaction behind the incorporation of more nitrogen into the E-CNDs could be attributed to the faster reaction between the amines of EDA with the carboxylic groups of citric acid, compared to formation of U-CNDs. The reaction between amides of urea and carboxylic groups of citric acid is slower due to the resonance from the double bonded carbon atoms of urea [58].

The zeta potential showed the surface charge of the E-CNDs and U-CNDs to be -7.32 ± 0.92 mV and -38.50 ± 2.72 mV, respectively. The more negative charge of the U-CNDs is attributed to the higher ratio of COO^- groups and the less negative charge of the E-CNDs to the presence of positive charged amine groups, which is in accordance with the XPS data. The FTIR (Fig. S4) spectra of both types of CNDs show broad absorption bands at 3000-3500 cm^{-1} assigned to stretching vibrations of O–H and N–H corresponding to the carboxylic acid and amine groups, respectively. The bands at 1538, 1432, and 1375 cm^{-1} of the E-CNDs can be assigned to the

bending vibrations of N–H, C–N, and C–H, respectively [59]. U-CNDs shows a peak at 1750 cm^{-1} which can be ascribed to the stretching frequencies of –C═O derived from –COOH. Similarly, C═C bending peak at 1549 cm^{-1} and characteristic O–H bending at 1655 cm^{-1} are observed [60]. The FTIR results clearly demonstrates the presence of amino, carboxyl and hydroxyl groups on the surface of the two CNDs, which attributes to the overall hydrophilicity of the CNDs.

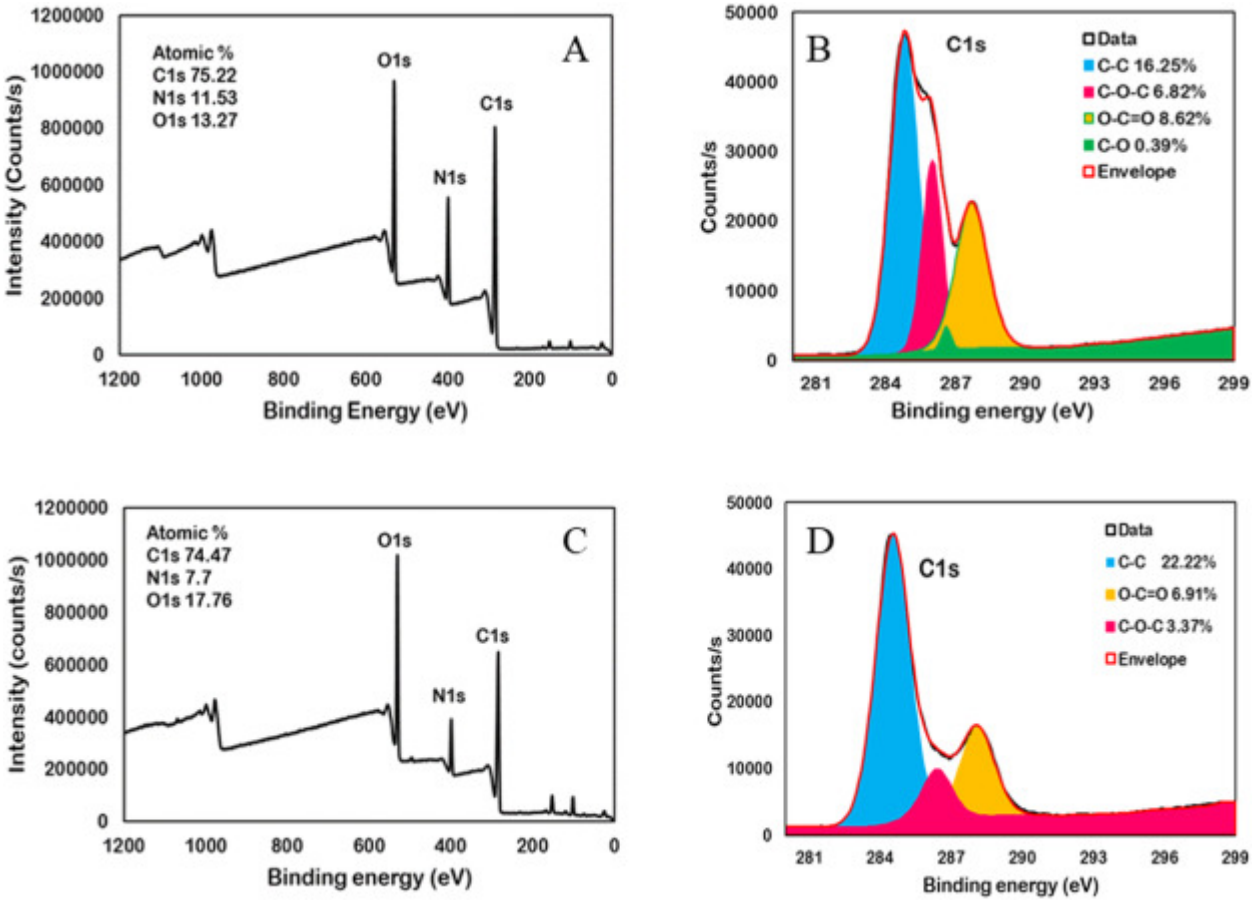

Fig. 2. XPS survey spectrum of E-CNDs (A) and U-CNDs (C) respectively. High resolution C1s peaks of E-CNDs (B) and U-CNDs (D).

3.2. Optical properties of CNDs

The UV–Visible spectrum of E-CNDs (Fig. 3A) and U-CNDs (Fig. 3B) shows shoulder peaks at 250 nm and 245 nm which are attributed to π- π* transitions of C═C (aromatic sp^2 domains) [61]. Strong broad peaks at 350 nm and 337 nm are assigned to n-π transitions of C═O bond involving functional groups with electron lone pairs on the E-CNDs and U-CNDs respectively [40]. The strong emission peaks of the E-CNDs (Fig 3A) and U-CNDs (Fig. 3B) are centered at ~450 nm with an excitation wavelength of 350 nm. Both the CNDs exhibit yellow/brown color under daylight and emitted blue light under UV light irradiation (Fig. 3A & B inset). The excitation dependence emission of E-CNDs and U-CNDs is observed at different wavelengths starting from 330 to 450 nm with an increment of 30 nm (Fig. S5), which may be due to the fluorescence origin of the CNDs relevant to the sizes, surface states, and functional groups. The

strongest emission peak is observed at an excitation wavelength of 350 nm for E-CNDs [62]. With the U-CNDs, strong emission peaks, but less than that of E-CNDs, were observed at broad range of (360–420 nm) excitation wavelengths which correspond to the broad absorption spectrum (Fig. 3B). The highest quantum yields of E-CNDs and U-CNDs are measured to be 64.0 ± 1.2% and 8.4 ± 0.7%, respectively, with reference to quinine sulfate [63].

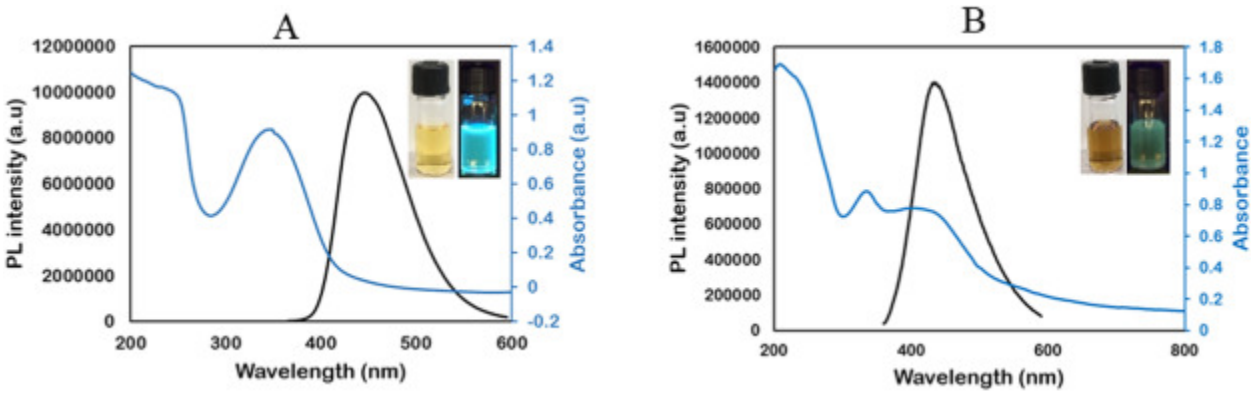

Fig. 3. UV–Vis absorption (blue) and PL emission (black) of E-CNDs (0.01 mg mL^{-1}) (A) and U-CNDs (0.1 mg mL^{-1}) (B). (For interpretation of the references to color in this figure legend, the reader is referred to the Web version of this article.)

3.3. Fluorescence sensing of Fe (III) ions

The fluorescence intensity of both the E-CNDs (Fig. S6A) and U-CNDs (Fig. S6B) quenches rapidly within 30 s upon addition of Fe (III) ions (60 μM). The excitation wavelength was 350 nm for this experiment. At the time frame of 1 min, the decrease in the fluorescence intensity stabilized and no significant change in the fluorescence intensity was observed even after 15 min. This clearly shows that the CNDs can be used as a fluorescent probe in the detection of Fe (III) ions rapidly within a minute. Note that no significant change is observed in the absorption spectra of E-CNDs (Fig. S7A) and U-CNDs (Fig. S7B) after the addition of Fe (III) (100 μM) ions.

Fig. 4A and 4B are clearly evidence that, with increase in the concentration of Fe (III) (from top to bottom: 0, 1, 2, 5, 10, 20, 50, 100, 200, 500, 1000, 2000, 5000 μM), the fluorescence intensity of both the E-CNDs and U-CNDs decreased significantly with concentration increase of Fe (III). Moreover, there is a linear correlation between the quenching efficiency ($(F_0–F)/F$) and Fe (III) ion concentration in both E-CNDs (Fig. 4C) and U-CNDs (Fig. 4D), where F_0 and F represent the fluorescence intensity of the CNDs in the absence and presence of Fe (III) ions, respectively. The limit of detection (LOD) is calculated using the signal noise ratio S/N = 3 for the CNDs based on the plots with the low concentration below sub μM (Fig. S8). The LOD is determined to be 18 nM and 30 nM for E-CNDs and U-CNDs, respectively. Table S1 lists a number of publications using CNDs as PL probes for Fe (III) detection for a comparison to this work. This work demonstrates good performance for Fe (III) detection in terms of the lowest detection limit, sensitivity and a much larger dynamic detection range at the similar level of quantum yield to the best performance in literature, such as in Refs. [[40], [41], [42],64,65].

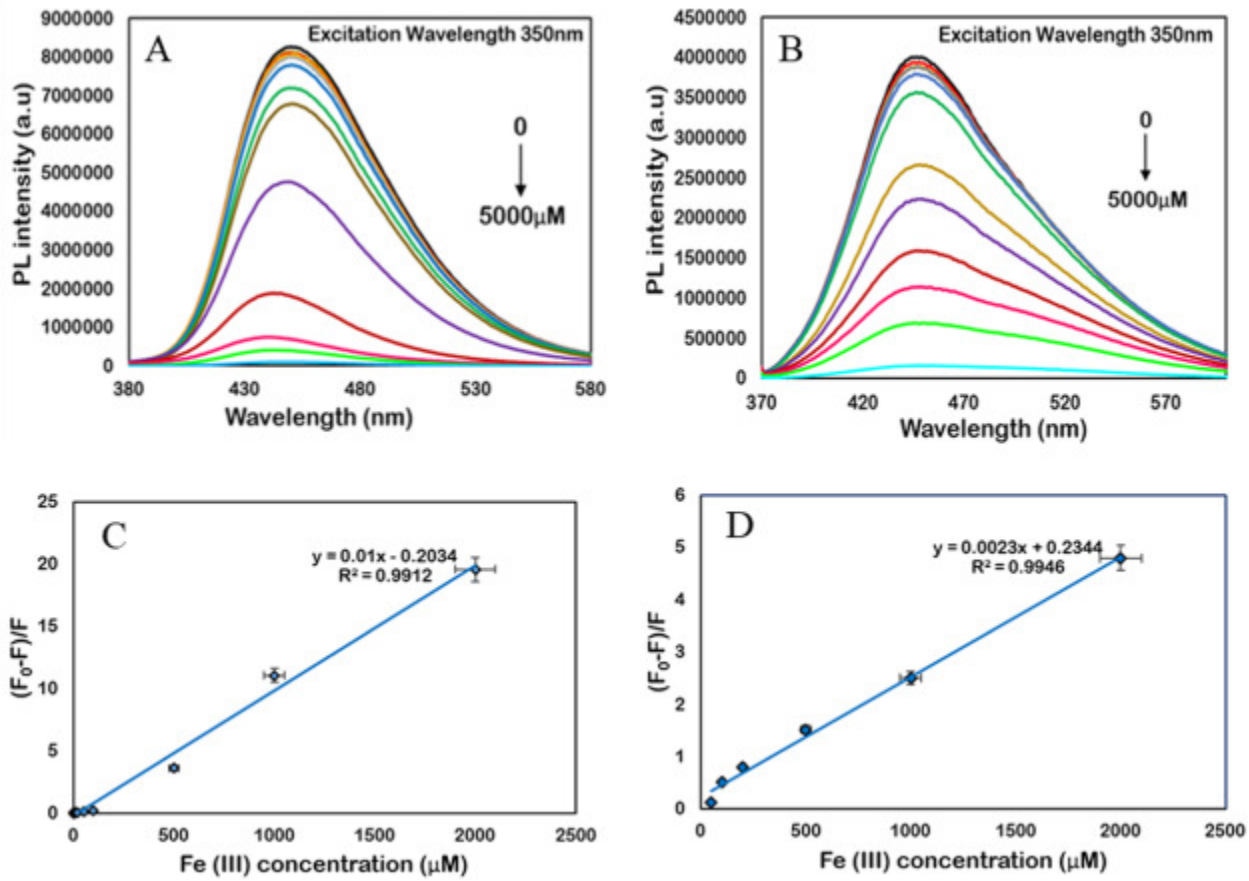

Fig. 4. PL intensity of E-CNDs (0.01 mg mL^{-1}) (A) and U-CNDs (0.1 mg mL^{-1}) (B) upon addition of different concentrations of Fe (III) ions. Linear plot of E-CNDs (C) and U-CNDs (D) fluorescence quenching, (F_0–F)/F, versus Fe (III) concentration at 0.5–2000 μM for E-CNDs and 1.0–2000 μM for U-CNDs. Lower concentrations of Fe (III) are ploted in Fig. S8.

3.4. Stability and selectivity of the CNDs

The stability of the E-CNDs (Fig. 5A) & U-CNDs (Fig. 5B) was observed for 50 days with an interval of 10 days at a concentration of 0.05 mg mL^{-1}. There is no significant decrease in the fluorescence intensity in both types of CNDs. This suggests the stability of the CNDs in the aqueous solution, which can be a better entity for use in biological solutions. The selectivity of the CNDs towards different metal ions (Ca^{2+}, Co^{2+}, Fe^{2+}, Ag^{+}, Cu^{2+}, K^{+}, Fe^{3+}, Cr^{3+}, and Mg^{2+}) of 50 μM concentration was demonstrated using fluorescence spectroscopic measurements. Both E-CNDs (0.05 mg mL^{-1}) (Fig 5C) and U-CNDs (0.1 mg mL^{-1}) (Fig. 5D) show significant decrease in the fluorescence intensity upon addition of Fe (III) ions in comparison to the other metal ions. The quenching efficiency of E-CNDs (Fig. S9A) and U-CNDs (Fig. S9B) towards Fe (III) was found to be 87 ± 4% and 70 ± 3%, respectively, much higher in comparison to other metal ions. The metal ions have no significant effect on the fluorescence quenching of E-CNDs (Fig. S9C) and U-CNDs (Fig. S9D), but in the presence of Fe (III) ions, the decrease in the intensity is obvious (Fig. 5E & F). Note that the counter anions, such as NO^{3-}, Cl^{-} in this study show insignificant interference. The insignificance of fluorescence interference with metal ions

suggests the high selectivity of both the CNDs as potential probes in the detection of Fe (III) ions.

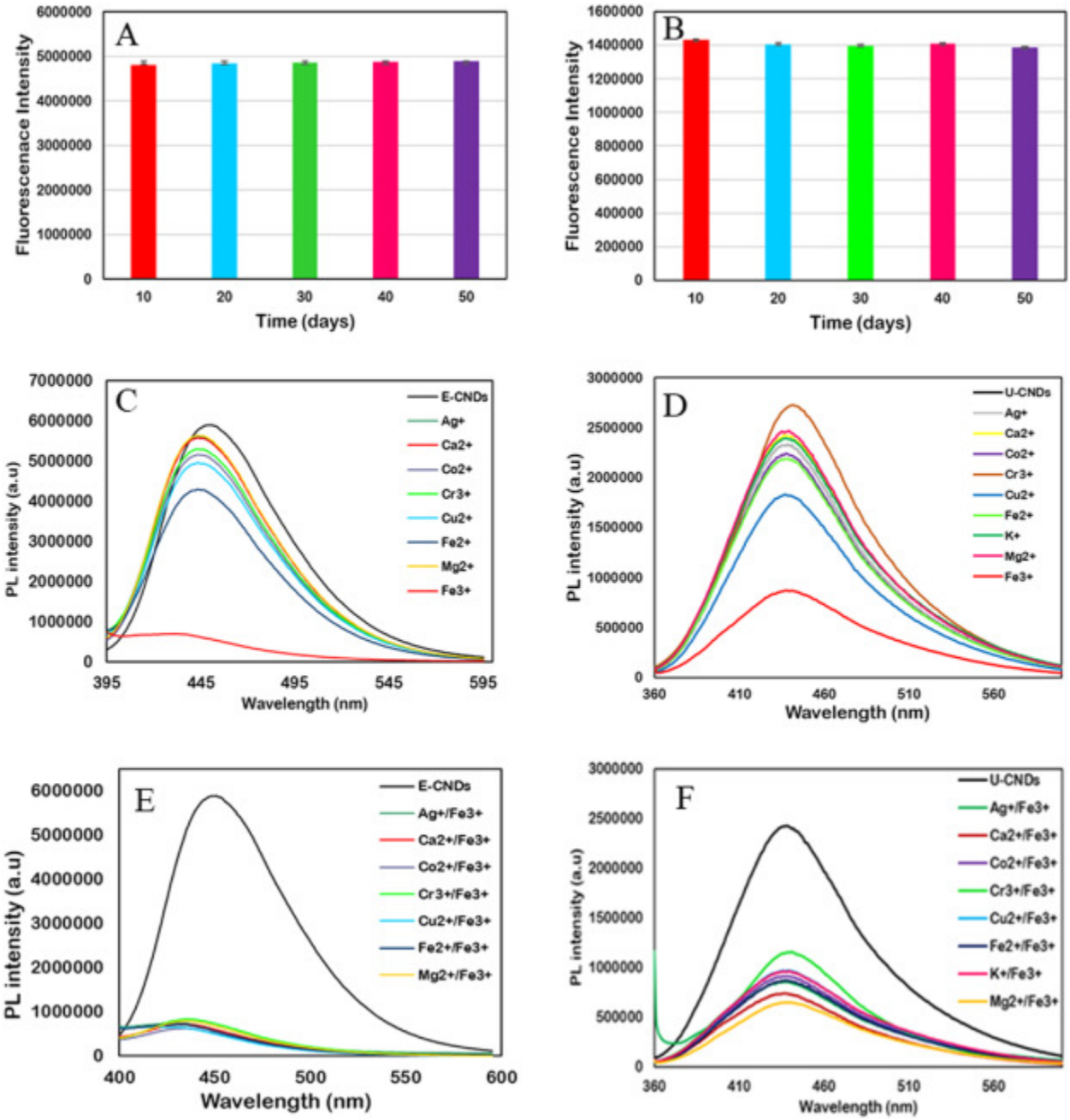

Fig. 5. Stability of fluorescence intensity of 0.05 mg mL^{-1} E-CNDs (A) & 0.1 mg mL^{-1} U-CNDs (B) with time (days). Representative fluorescence emission spectra of the E-CNDs (C) and U-CNDs (D) in presence of different cations at a concentration of 50 µM in water, and (E) E-CNDs and (F) U-CNDs with mixed 50 µM Fe (III) ions with different cations (50 µM).

3.5. Detection of iron in real samples

To demonstrate detection of Fe (III) in real samples, the iron content in both tap water and human serum samples were determined using the CNDs. When the E-CNDs (Fig. S10A) and U-CNDs (Fig. S10B) were added to the tap water and human serum, there is a decrease in the fluorescent intensity which indicated the presence of iron. With the help of the calibration curve between Fe (III) concentration and the CNDs fluorescence intensity, E-CNDs and U-CNDs were able to detect the iron content in tap water to be 3.8 μM and 1 μM, respectively. The iron content in concentrated human serum sample was found to be 27.8 μM and 24.6 μM using E-CNDs and U-CNDs, respectively. The ability of the CNDs to detect the iron content in real samples was validated with inductively coupled plasma optical emission spectrophotometer (ICP OES). Standard solutions of Fe (III) (0.1, 1, 5, 10 ppm) were prepared and a calibration curve was plotted with Fe (III) concentration vs. emission intensity (Fig. S11). Samples of tap water and serum in 3% HNO_3 were analyzed with ICP for iron content and was found to be 2.56 μM and 28 μM respectively which is in accordance with the fluorescence data of the CNDs (Fig. 4).

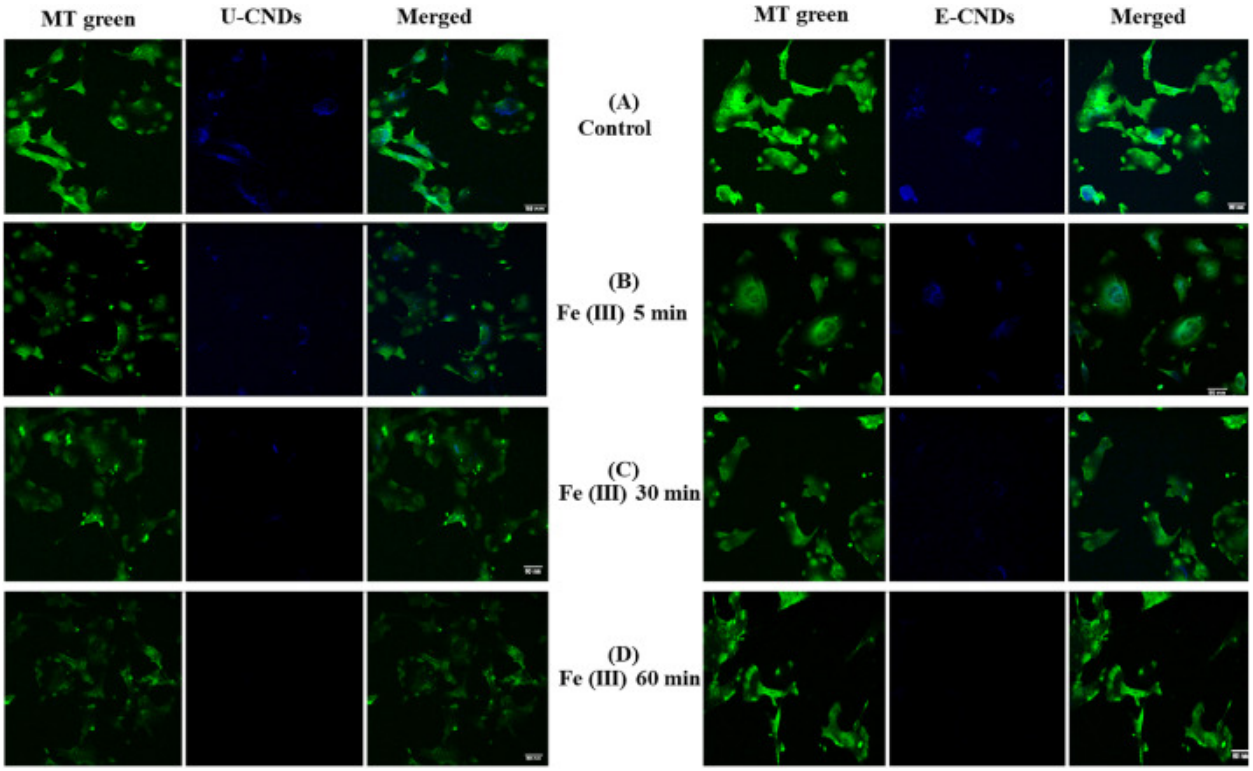

Fig. 6. Fluorescence images of EA. hy926 cells incubated with E-CNDs (0.1 mg mL^{-1}, right) and U-CNDs (0.3 mg mL^{-1}, left) in the absence of Fe (III) ions (A). Fluorescence images of EA. hy926 cells incubated with E-CNDs and U-CNDs in the presence of 10 μM of Fe (III) for different time intervals of 5 min (B), 30 min (C) and 1 h (D).

3.6. Optical sensing of Fe (III) in living cells

The high quantum yield and excellent photostability allow the as-synthesized CNDs to be used in bioimaging. The confocal images show the localization of both the CNDs inside the EA. hy926 cells with bright blue fluorescence (Fig. 6). The cells were counter stained with Mito-tracker green (MT green) to label the actin filaments. In the absence of Fe (III) ions, no quenching of fluorescence intensity is observed in the cells incubated with either E-CNDs or U-

CNDs (Fig. 6A). Quenching of fluorescence is observed in the cells incubated with the CNDs upon the addition of Fe (III) ions. At time interval of 5 min, there is not much decrease in the fluorescence intensity when compared to the control (Fig. 6B), but after the incubation of Fe (III) ions for 30 min, there is a significant decrease in the fluorescence intensity (Fig. 6C). The fluorescence is almost completely quenched after incubation of Fe (III) ions for 1 h (Fig. 6D).

3.7. Fluorescence quenching reaction and electrochemistry of Fe (III) with CNDs

The possible quenching mechanism of the CNDs in presence of Fe (III) ions was investigated. The quenching process may occur due to the formation of a non-fluorescent complex, when a fluorescent molecule and a quencher interact together. The process can either be static or dynamic quenching which can be fitted to the Stern-Volmer equation [66].

$$F_0/F = 1 + \mathrm{K}_{sv}[Q] \quad (2)$$

where F_0 and F represent the fluorescence intensity of the CNDs in the absence and presence of Fe (III) ions, respectively, K_{sv} is the quenching constant, and Q is the concentration of the quencher (Fe (III) ions).

Both the CNDs show good linear correlation with the Fe (III) ion concentration following the Stern-Volmer plot. The quenching constant (K_{sv}) for the low concentration linear range (0.01–0.5 μM) was determined to be $5.57 \times 10^4\ M^{-1}$ and $3.76 \times 10^4\ M^{-1}$ for E-CNDs (Fig. S8A) and U-CNDs (Fig. S8B), respectively, by plotting the quenching efficiency ((F_0–F)/F) vs. Fe (III) ion concentration. The K_{sv} values for E-CNDs (Fig 4C) and U-CNDs (Fig. 4D) was calculated as $1 \times 10^4\ M^{-1}$ and $2.3 \times 10^3\ M^{-1}$, respectively, for the broader linear concentration range of 0.5–2000 μM. The larger constant K_{sv} value suggests faster kinetics of the association of CNDs with Fe (III) at lower concentration of CNDs. Upon addition of Fe (III) ions to the CNDs solution, the strong blue fluorescence was quenched which was clearly evident from the decrease in the fluorescence intensity spectra of both the CNDs (Fig. 4A & B). In the presence of Fe (III) ions, the fluorescence intensity of the CNDs was quenched but this phenomenon was not observed upon the addition of Fe (II) ions (Fig. S12). In the presence of Fe (III) ions, the nitrogen rich CNDs may donate an electron to the Fe (III) to an orbital in the half-filled d-shell, resulting in the formation of a low or non-fluorescent complex. Hence, a fluorescence quenching reaction is proposed that addition of CNDs to Fe (III) solution will form a complex of CNDs-Fe (III), then followed with electron transfer between the optical active sites of CNDs and Fe (III) ions where the Fe (III) is being reduced to Fe (II). As a result, the fluorescence of CNDs in the complex CNDs-Fe (III)/(II) is quenched.

To further verify the proposed charge transfer quenching process, electrochemistry using cyclic voltammograms (CV) of Fe (III) ions in the presence and absence of CNDs was performed with the potential window of −0.2 to 0.9 V vs. Ag/AgCl. The CV plots of Fe (III) ions have both oxidation and reduction peaks, but the peaks started to decrease upon the addition of the CNDs. Moreover, the redox peaks disappeared with the increasing concentration of the CNDs (Fig. 7). This clearly states that, as the concentration of the CNDs increased and more CNDs-Fe (III) complex formation, electrons from the CNDs are being transferred to the Fe (III) ions resulting in the loss of redox peaks. The CVs for E-CNDs present much more decrease in peak current

than that of U-CNDs, even though the concentration of E-CNDs is much lower. The results strongly support that the fluorescence of E-CNDs quenching reaction is kinetically faster than the U-CNDs by Fe (III), a good agreement with the K_{sv} value obtained by the Stern-Volmer equation. Based on the observation, a quenching reaction of E-CNDs with Fe (III) is as follows:

$$E - CND + n(Fe(\mathrm{III})) \rightarrow E - CND - (Fe(\mathrm{III}))_n \leftrightarrow E - CND - (Fe(\mathrm{II}))_n \qquad (3)$$

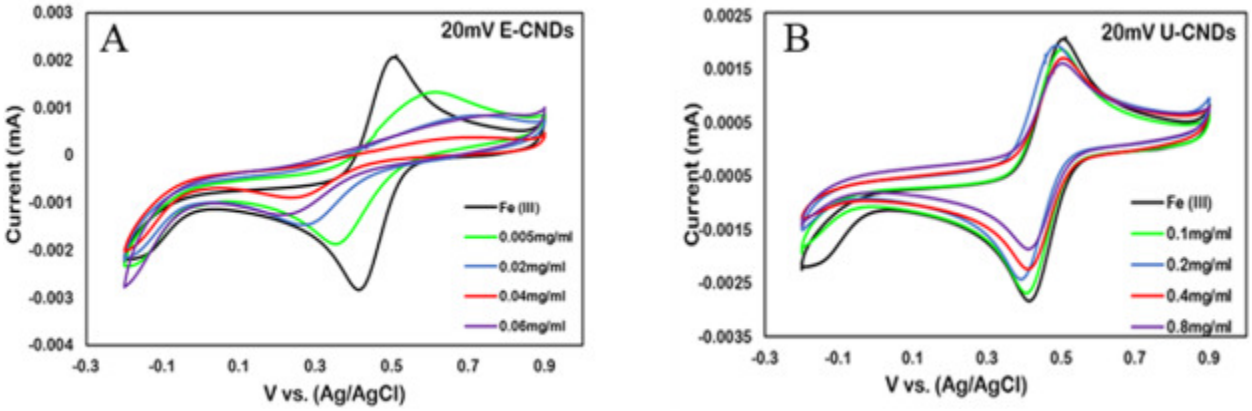

Fig. 7. Cyclic voltammograms of Fe (III) incubated with different concentrations of E-CNDs (A) and U-CNDs (B) at a scan rate of 20 mV s^{-1}.

The n in Eq. (3) is the stoichiometric coefficient (a number greater than 1) of Fe ions combine to a single CND through coordinating or chelating interactions due to large number of surface functional groups for chelating [67]. When CNDs are added to the Fe (III) solution, a complex E-CND-(Fe (III))$_n$ forms and participates in the redox reaction at the working electrode, resulting in E-CND-(Fe (II))$_n$ complex. Note that, since the Fe (III) molar concentration is orders higher than the CNDs, not all Fe (III) ions form the CND-Fe (III) complex. The CV redox peaks represent an ensemble of both the free iron ions and the complex (Fig. 7). Due to the association of E-CNDs with Fe (II) after the reaction, the diffusion of E-CND-(Fe(II))$_n$ complex to the working electrode is slower than the free iron ions in the cyclic voltammetry, consequently a broadened oxidation peak of Fe (II) in the CVs is observed. The larger separation of oxidation and reduction peaks with more CNDs in the solution suggests slower electrochemical kinetics of redox reaction of CND-(Fe (III))$_n$/CND-n(Fe (II))$_n$ at the electrode surface because of more CNDs-(Fe (II/III))$_n$ complex formation and less free Fe (III) ions in the solution [68]. In a control experiment, the cyclic voltammetry of Fe (II) treated with E-CNDs or U-CNDs presents insignificant changes of the redox reaction at electrode surfaces (Figs. S13 and S14), suggesting that the chelating of CNDs to Fe (II) is weak and electron transfer from Fe (II) to CNDs is not in favor. This result indicates the fluorescence quenching would be specifically electron transfer from the CNDs to Fe (III) ions when the complex forms, namely oxidation of CNDs and reduction of Fe (III) promoted by applied external voltage. Moreover, this control experiment also implies that it is unlikely the adhesion of CNDs or a contamination to the electrode surface to cause the slower electrochemical kinetics.

The selectivity of the CNDs can be attributed to the energy level match between the photo-excited excitons (PL centers) in CNDs and the level of valence d state orbit of the Fe (III) when the CND- (Fe(III))$_n$ complex forms, resulting the reduction of Fe(III) [67,69]. In this work, the

Fe (III) valence d state level as an electron acceptor matches the CNDs' PL centers, similar to Ref. [67] for Fe (III) detection, while other metal ions don't, though CNDs might be able to form a complex with other metal ions via chelating interactions. This can be further elucidated by the difference of standard reduction potential of metal ions. For instance, the standard reduction potential of Fe (III) to Fe (II) and Cu (II) to Cu (I) are 0.77 V (NHE) and 0.16 V (NHE), respectively. The Fe (III) is a much stronger oxidizing agent (electron acceptor) than Cu (II). Hence, one should not expect strong fluorescence quenching with addition of Cu (II) in this case, though the CNDs-Cu (II) complex may form due to the presence of amine groups of CNDs. This was confirmed by the CVs of Cu^{2+} in water with and without addition of E-CNDs (Fig. S15) or U-CNDs (Fig. S16), which don't show significant changes in shape of the CVs while the redox peak currents decrease with addition of CNDs due to formation of CND- $(Cu(II)_n$, which indicates decrease of free Cu^{2+}. Similarly, this principle is applicable to other metal ions that their energy levels don't match the excitons (PL centers) in CNDs for charge transfer. As a result, no significant interference was observed from Ca^{2+}, Co^{2+}, Fe^{2+}, Ag^{+}, Cu^{2+}, K^{+}, Fe^{3+}, Cr^{3+} and Mg^{2+} *etc*.

4. Conclusion

In summary, E-CNDs and U-CNDs synthesized using one step microwave synthesis are able to detect Fe (III) ions with high selectivity and sensitivity. The synthesized CNDs show good aqueous solubility, excellent stability, and high PL with E-CNDs quantum yield as high as 64%. A decrease in fluorescence intensity is observed with the increase of Fe (III) ions in the CND solution. E-CND probes provide higher sensitive analysis of Fe (III) ions in comparison to U-CNDs probe with limit of detection of about 18 nM for E-CNDs and 30 nM for U-CNDs, owing to increase nitrogen content in E-CNDs. The CNDs are used as probes to detect Fe (III) in real samples such as tap water and human serum without pretreatment, and the results are validated by ICP element analysis. Both the CNDs are successfully internalized inside endothelial cells with bright blue fluorescence and the phenomenon of fluorescence quenching is observed when the cells are incubated with Fe (III), suggesting potential sensing of Fe (III) in living cells. The fluorescence quenching of CNDs is attributed to a charge transfer mechansim specifically between CNDs to Fe (III) which is further verified in the cyclic voltammetry studies. The energy match of the excitons (PL centers) of the CNDs for electron transfer to the metal ions is critical for allowed charge transfer quenching mechanism when the CNDs-metal ion complex forms. In conclusion, these CNDs can be valuable nanoprobes in the sensitive and selective detection of Fe (III) ions in a broad dynamic range concentration (0–2000 μM).

Funding
This work is partially supported by the US National Science Foundation (NSF) (Award#: 1832134), and a North Carolina State fund through the Joint School of Nanoscience and Nanoengineering (JSNN), a joint institution between The University of North Carolina – Greensboro and North Carolina A&T State University.

Declaration of interest statement
We declare that we have no financial and personal relationships with other people or organizations that can inappropriately influence our work, there is no professional or other personal interest of any nature or kind in any product, service and/or company that could be

construed as influencing the position presented in, or the review of, the manuscript entitled, "High Quantum Yield Fluorescent Carbon Nanodots for Detection of Fe (III) Ions and Electrochemical Study of Quenching Mechanism".

Acknowledgements
The research was conducted at the Joint School of Nanoscience and Nanoengineering, a member of Southeastern Nanotechnology Infrastructure Corridor (SENIC) and National Nanotechnology Coordinated Infrastructure (NNCI), which is supported by the US National Science Foundation (ECCS-1542174).

Appendix A. Supplementary data
Supplementary data to this article can be found online at https://doi.org/10.1016/j.talanta.2019.120538.

References

[1] J. Anastassopoulou, Metal–DNA interactions, J. Mol. Struct. 651–653 (2003) 19–26.

[2] S.R. Lynch, Interaction of iron with other nutrients, Nutr. Rev. 55 (4) (1997) 102–110.

[3] P.T. Lieu, M. Heiskala, P.A. Peterson, Y. Yang, The roles of iron in health and disease, Mol. Asp. Med. 22 (1–2) (2001) 1–87.

[4] N. Abbaspour, R. Hurrell, R. Kelishadi, Review on iron and its importance for human health, J. Res. Med. Sci. 19 (2) (2014) 164–174.

[5] S.L. Helman, G.J. Anderson, D.M. Frazer, Dietary iron absorption during early postnatal life, Biometals 32 (2019) s10534-019-00181-9.

[6] P.H. Rosenzweig, S.L. Volpe, Iron, thermoregulation, and metabolic rate, Crit. Rev. Food Sci. Nutr. 39 (2) (1999) 131–148.

[7] J. Kaplan, D.M. Ward, Muscle specific iron deficiency has systemic consequences, EBioMedicine 2 (11) (2015) 1582–1583.

[8] L. Silvestri, C. Camaschella, A potential pathogenetic role of iron in Alzheimer's disease, J. Cell Mol. Med. 12 (5A) (2008) 1548–1550.

[9] T. Hirayama, H. Nagasawa, Chemical tools for detecting Fe ions, J. Clin. Biochem. Nutr. 60 (1) (2017) 39–48.

[10] K.P. Carter, A.M. Young, A.E. Palmer, Fluorescent sensors for measuring metal ions in living systems, Chem. Rev. 114 (8) (2014) 4564–4601.

[11] U. Resch-Genger, M. Grabolle, S. Cavaliere-Jaricot, R. Nitschke, T. Nann, Quantum dots versus organic dyes as fluorescent labels, Nat. Methods 5 (9) (2008) 763–775.

[12] A. Lesiak, K. Drzozga, J. Cabaj, M. Banski, K. Malecha, A. Podhorodecki, Optical sensors based on II-VI quantum dots, Nanomaterials 9 (2) (2019) 192.

[13] R. Hardman, A toxicologic review of quantum dots: toxicity depends on physicochemical and environmental factors, Environ. Health Perspect. 114 (2) (2006) 165–172.

[14] A. Valizadeh, H. Mikaeili, M. Samiei, S.M. Farkhani, N. Zarghami, M. Kouhi, A. Akbarzadeh, S. Davaran, Quantum dots: synthesis, bioapplications, and toxicity, Nanoscale Res. Lett. 7 (1) (2012) 480-480.

[15] W.H. Chan, N.H. Shiao, Cytotoxic effect of CdSe quantum dots on mouse embryonic development, Acta Pharmacol. Sin. 29 (2) (2008) 259–266.

[16] S.S. Agasti, S. Rana, M.-H. Park, C.K. Kim, C.-C. You, V.M. Rotello, Nanoparticles for detection and diagnosis, Adv. Drug Deliv. Rev. 62 (3) (2010) 316–328.

[17] N.L. Rosi, C.A. Mirkin, Nanostructures in biodiagnostics, Chem. Rev. 105 (4) (2005) 1547–1562.

[18] S.N. Baker, G.A. Baker, Luminescent carbon nanodots: emergent nanolights, Angew. Chem. Int. Ed. 49 (38) (2010) 6726–6744.

[19] X.T. Zheng, A. Ananthanarayanan, K.Q. Luo, P. Chen, Glowing graphene quantum dots and carbon dots: properties, syntheses, and biological applications, Small 11 (14) (2015) 1620–1636.

[20] M. Ahmed, M. Faisal, A. Ihsan, M.M. Naseer, Fluorescent organic nanoparticles (FONs) as convenient probes for metal ion detection in aqueous medium, Analyst 144 (2019) 2480–2497.

[21] S. Zhu, Y. Song, X. Zhao, J. Shao, J. Zhang, B. Yang, The photoluminescence mechanism in carbon dots (graphene quantum dots, carbon nanodots, and polymer dots): current state and future perspective, Nano Res 8 (2) (2015) 355–381.

[22] M. Zheng, Z. Xie, D. Qu, D. Li, P. Du, X. Jing, Z. Sun, On–off–on fluorescent carbon dot nanosensor for recognition of chromium(VI) and ascorbic acid based on the inner filter effect, ACS Appl. Mater. Interfaces 5 (24) (2013) 13242–13247.

[23] Z. Zeng, W. Zhang, D.M. Arvapalli, B. Bloom, A. Sheardy, T. Mabe, Y. Liu, Z. Ji, H. Chevva, D.H. Waldeck, J. Wei, A fluorescence-electrochemical study of carbon nanodots (CNDs) in bio- and photoelectronic applications and energy gap investigation, Phys. Chem. Chem. Phys. 19 (30) (2017) 20101–20109.

[24] S.C. Ray, A. Saha, N.R. Jana, R. Sarkar, Fluorescent carbon nanoparticles: synthesis, characterization, and bioimaging application, J. Phys. Chem. C 113 (43) (2009) 18546–18551.

[25] P. Roy, P.-C. Chen, A.P. Periasamy, Y.-N. Chen, H.-T. Chang, Photoluminescent carbon nanodots: synthesis, physicochemical properties and analytical applications, Mater, Today 18 (8) (2015) 447–458.

[26] W. Wei, C. Xu, J. Ren, B. Xu, X. Qu, Sensing metal ions with ion selectivity of a crown ether and fluorescence resonance energy transfer between carbon dots and graphene, Chem. Commun. 48 (9) (2012) 1284–1286.

[27] B. Kong, A. Zhu, C. Ding, X. Zhao, B. Li, Y. Tian, Carbon dot-based inorganic-organic nanosystem for two-photon imaging and biosensing of pH variation in living cells and tissues, Adv. Mater. 24 (43) (2012) 5844–5848.

[28] S. Hu, A. Trinchi, P. Atkin, I. Cole, Tunable photoluminescence across the entire visible spectrum from carbon dots excited by white light, Angew. Chem. Int. Ed. 54 (10) (2015) 2970–2974.

[29] H.U. Lee, S.Y. Park, E.S. Park, B. Son, S.C. Lee, J.W. Lee, Y.-C. Lee, K.S. Kang, M.I. Kim, H.G. Park, S. Choi, Y.S. Huh, S.-Y. Lee, K.-B. Lee, Y.-K. Oh, J. Lee, Photoluminescent carbon nanotags from harmful cyanobacteria for drug delivery and imaging in cancer cells, Sci. Rep. 4 (2014) 4665.

[30] X. Sun, Y. Lei, Fluorescent carbon dots and their sensing applications, Trends Anal. Chem. 89 (2017) 163–180.

[31] G. He, M. Xu, M. Shu, X. Li, Z. Yang, L. Zhang, Y. Su, N. Hu, Y. Zhang, Rapid solid-phase microwave synthesis of highly photoluminescent nitrogen-doped carbon dots for Fe3+ detection and cellular bioimaging, Nanotechnology 27 (39) (2016) 395706.

[32] K.K. Karali, L. Sygellou, C.D. Stalikas, Highly fluorescent N-doped carbon nanodots as an effective multi-probe quenching system for the determination of nitrite, nitrate and ferric ions in food matrices, Talanta 189 (2018) 480–488.

[33] K.M. Omer, D.I. Tofiq, A.Q. Hassan, Solvothermal synthesis of phosphorus and nitrogen doped carbon quantum dots as a fluorescent probe for iron(III), Microchim. Acta 185 (10) (2018) 466.

[34] L. Rao, Y. Tang, Z. Li, X. Ding, G. Liang, H. Lu, C. Yan, K. Tang, B. Yu, Efficient synthesis of highly fluorescent carbon dots by microreactor method and their application in Fe3+ ion detection, Mater. Sci. Eng. C Mater. Biol. Appl. 81 (2017) 213–223.

[35] Q. Ye, F. Yan, Y. Luo, Y. Wang, X. Zhou, L. Chen, Formation of N, S-codoped fluorescent carbon dots from biomass and their application for the selective detection of mercury and iron ion, Spectrochim. Acta A Mol. Biomol. Spectrosc. 173 (2017) 854–862.

[36] J. Feng, Y. Chen, Y. Han, J. Liu, C. Ren, X. Chen, Fluorescent carbon nanoparticles: a low-temperature trypsin-assisted preparation and Fe3+ sensing, Anal. Chim. Acta 926 (5) (2016) 107–117.

[37] Y. Song, C. Zhu, J. Song, H. Li, D. Du, Y. Lin, Drug-derived bright and color-tunable N-doped carbon dots for cell imaging and sensitive detection of Fe3+ in living cells, ACS Appl. Mater. Interfaces 9 (8) (2017) 7399–7405.

[38] C. Li, Y. Wang, X. Zhang, X. Guo, X. Kang, L. Du, Y. Liu, Red fluorescent carbon dots with phenylboronic acid tags for quick detection of Fe(III) in PC12 cells, J. Colloid Interface Sci. 526 (2018) 487–496.

[39] J. Zhang, J. Yan, Y. Wang, Y. Zhang, One-step hydrothermal approach to synthesis carbon dots from D-sorbitol for detection of iron(III) and cell imaging, J. Nanosci. Nanotechnol. 18 (7) (2018) 4457–4463.

[40] B. Shi, Y. Su, L. Zhang, M. Huang, R. Liu, S. Zhao, Nitrogen and phosphorus Codoped carbon nanodots as a novel fluorescent probe for highly sensitive detection of Fe3+ in human serum and living cells, ACS Appl. Mater. Interfaces 8 (17) (2016) 10717–10725.

[41] H. Zhang, Y. Chen, M. Liang, L. Xu, S. Qi, H. Chen, X. Chen, Solid-Phase synthesis of highly fluorescent nitrogen-doped carbon dots for sensitive and selective probing ferric ions in living cells, Anal. Chem. 86 (19) (2014) 9846–9852.

[42] S. Li, Y. Li, J. Cao, J. Zhu, L. Fan, X. Li, Sulfur-doped graphene quantum dots as a novel fluorescent probe for highly selective and sensitive detection of Fe3+, Anal. Chem. 86 (20) (2014) 10201–10207.

[43] F. Du, X. Gong, W. Lu, Y. Liu, Y. Gao, S. Shuang, M. Xian, C. Dong, Bright-green-emissive nitrogen-doped carbon dots as a nanoprobe for bifunctional sensing, its logic gate operation and cellular imaging, Talanta 179 (2018) 554–562.

[44] C. Sarkar, A.R. Chowdhuri, A. Kumar, D. Laha, S. Garai, J. Chakraborty, S.K. Sahu, One pot synthesis of carbon dots decorated carboxymethyl cellulose- hydroxyapatite nanocomposite for drug delivery, tissue engineering and Fe3+ ion sensing, Carbohydr. Polym. 181 (2018) 710–718.

[45] C. Wang, T. Hu, Z. Wen, J. Zhou, X. Wang, Q. Wu, C. Wang, Concentration-dependent color tunability of nitrogen-doped carbon dots and their application for iron(III) detection and multicolor bioimaging, J. Colloid Interface Sci. 521 (2018) 33–41.

[46] R. Patidar, B. Rebary, D.A. Sanghani, G.R. Bhadu, P. Paul, Fluorescent carbon nanoparticles obtained from charcoal via green methods and their application for sensing Fe3+ in an aqueous medium, Luminescence 32 (8) (2017) 1466–1472.

[47] P. Suvarnaphaet, C.S. Tiwary, J. Wetcharungsri, S. Porntheeraphat, R. Hoonsawat, P.M. Ajayan, I.M. Tang, P. Asanithi, Blue photoluminescent carbon nanodots from limeade, Mater. Sci. Eng. C Mater. Biol. Appl. 69 (2016) 914–921.

[48] H. Li, F.-Q. Shao, S.-Y. Zou, Q.-J. Yang, H. Huang, J.-J. Feng, A.-J. Wang, Microwave-assisted synthesis of N,P-doped carbon dots for fluorescent cell imaging, Microchim. Acta 183 (2) (2016) 821–826.

[49] L. Wang, B. Li, L. Li, F. Xu, Z. Xu, D. Wei, Y. Feng, Y. Wang, D. Jia, Y. Zhou, Ultrahigh-yield synthesis of N-doped carbon nanodots that down-regulate ROS in zebrafish, J. Mater. Chem. B 5 (38) (2017) 7848–7860.

[50] D. Xiao, D. Yuan, H. He, J. Lu, Microwave-assisted one-step green synthesis of amino-functionalized fluorescent carbon nitride dots from chitosan, Luminescence 28 (4) (2013) 612–615.

[51] G. Liu, B. Li, Y. Liu, Y. Feng, D. Jia, Y. Zhou, Rapid and high yield synthesis of carbon dots with chelating ability derived from acrylamide/chitosan for selective detection of ferrous ions, Appl. Surf. Sci. 487 (2019) 1167–1175.

[52] L. Wang, B. Li, F. Xu, X. Shi, D. Feng, D. Wei, Y. Li, Y. Feng, Y. Wang, D. Jia, Y. Zhou, High-yield synthesis of strong photoluminescent N-doped carbon nanodots derived from hydrosoluble chitosan for mercury ion sensing via smartphone APP, Biosens. Bioelectron. 79 (2016) 1–8.

[53] S. Zhu, Q. Meng, L. Wang, J. Zhang, Y. Song, H. Jin, K. Zhang, H. Sun, H. Wang, B. Yang, Highly photoluminescent carbon dots for multicolor patterning, sensors, and bioimaging, Angew. Chem. Int. Ed. 52 (14) (2013) 3953–3957.

[54] X. Zhu, J. Wang, Y. Zhu, H. Jiang, D. Tan, Z. Xu, T. Mei, J. Li, L. Xue, X. Wang, Green emitting N,S-co-doped carbon dots for sensitive fluorometric determination of Fe(III) and Ag(I) ions, and as a solvatochromic probe, Microchim. Acta 185 (11) (2018) 510.

[55] X. Zhai, P. Zhang, C. Liu, T. Bai, W. Li, L. Dai, W. Liu, Highly luminescent carbon nanodots by microwave-assisted pyrolysis, Chem. Commun. 48 (64) (2012) 7955–7957.

[56] K.J. Mintz, Y. Zhou, R.M. Leblanc, Recent development of carbon quantum dots regarding their optical properties, photoluminescence mechanism, and core structure, Nanoscale 11 (11) (2019) 4634–4652.

[57] X. Gong, W. Lu, M.C. Paau, Q. Hu, X. Wu, S. Shuang, C. Dong, M.M.F. Choi, Facile synthesis of nitrogen-doped carbon dots for Fe3+ sensing and cellular imaging, Anal. Chim. Acta 861 (2015) 74–84.

[58] J. L. G. Wade, Organic Chemistry, 6 ed., Prentice Hall2005.

[59] Q. Hu, M.C. Paau, Y. Zhang, W. Chan, X. Gong, L. Zhang, M.M.F. Choi, Capillary electrophoretic study of amine/carboxylic acid-functionalized carbon nanodots, J. Chromatogr. A 1304 (2013) 234–240.

[60] S. Qu, X. Wang, Q. Lu, X. Liu, L. Wang, A biocompatible fluorescent ink based on water-soluble luminescent carbon nanodots, Angew. Chem. Int. Ed. 51 (49) (2012) 12215–12218.

[61] X. Zhu, Z. Zhang, Z. Xue, C. Huang, Y. Shan, C. Liu, X. Qin, W. Yang, X. Chen, T. Wang, Understanding the selective detection of Fe3+ based on graphene quantum dots as fluorescent probes: the ksp of a metal hydroxide-assisted mechanism, Anal. Chem. 89 (22) (2017) 12054–12058.

[62] Y. Dong, H. Pang, H.B. Yang, C. Guo, J. Shao, Y. Chi, C.M. Li, T. Yu, Carbon-based dots co-doped with nitrogen and sulfur for high quantum yield and excitation-independent emission, Angew. Chem. Int. Ed. 52 (30) (2013) 7800–7804.

[63] C.A. Heller, R.A. Henry, B.A. McLaughlin, D.E. Bliss, Fluorescence spectra and quantum yields. Quinine, uranine, 9,10-diphenylanthracene, and 9,10-bis(phenylethynyl) anthracenes, J. Chem. Eng. Data 19 (3) (1974) 214–219.

[64] Y. Liu, W. Duan, W. Song, J. Liu, C. Ren, J. Wu, D. Liu, H. Chen, Red emission B, N, S-co-Doped carbon dots for colorimetric and fluorescent dual mode detection of Fe3+ ions in complex biological fluids and living cells, ACS Appl. Mater. Interfaces 9 (14) (2017) 12663–12672.

[65] X. Zhou, G. Zhao, X. Tan, X. Qian, T. Zhang, J. Gui, L. Yang, X. Xie, Nitrogen-doped carbon dots with high quantum yield for colorimetric and fluorometric detection of ferric ions and in a fluorescent ink, Microchim. Acta 186 (2) (2019) 67.

[66] H. Boaz, G.K. Rollefson, The quenching of fluorescence. Deviations from the stern-volmer law, J. Am. Chem. Soc. 72 (8) (1950) 3435–3443.

[67] Y. Wang, Q. Chang, S. Hu, Carbon dots with concentration-tunable multicolored photoluminescence for simultaneous detection of Fe3+ and Cu2+ ions, Sens. Actuators B Chem. 253 (2017) 928–933.

[68] J. Wei, H. Liu, A.R. Dick, H. Yamamoto, Y. He, D.H. Waldeck, Direct wiring of cytochrome c's heme unit to an Electrode: electrochemical studies, J. Am. Chem. Soc. 124 (32) (2002) 9591–9599.

[69] X. Gao, C. Du, Z. Zhuang, W. Chen, Carbon quantum dot-based nanoprobes for metal ion detection, J. Mater. Chem. C 4 (29) (2016) 6927–6945.